Effect of Multiple Alkanethiol Ligands on Solubility and Sintering Temperature of Gold Nanoparticles

Kevin Wang

Electrical Engineering and Computer Sciences
University of California at Berkeley

Technical Report No. UCB/EECS-2010-86
http://www.eecs.berkeley.edu/Pubs/TechRpts/2010/EECS-2010-86.html

May 25, 2010

Effect of Multiple Alkanethiol Ligands on Solubility and Sintering Temperature of Gold Nanoparticles

by

Kevin Wang

Research Project

Submitted to the Department of Electrical Engineering and Computer Sciences, University of California at Berkeley, in partial satisfaction of the requirements for the degree of **Master of Science, Plan II**.

Approval for the Report and Comprehensive Examination:

Committee:

Professor Vivek Subramanian
Research Advisor

(Date)

* * * * * * *

Professor Ali Javey
Second Reader

(Date)

Effect of Multiple Alkanethiol Ligands on Solubility and Sintering Temperature of Gold Nanoparticles

by

Kevin Wang

Master of Science – Electrical Engineering and Computer Sciences

May 10, 2010, University of California, Berkeley

Professor Vivek Subramanian, Advisor

Abstract

Printed electronics are a promising means for the manufacture of low cost electronics, but an improved printed conductor material must be developed. Metal nanoparticle-based inks provide the benefit of low sintering temperature, and achieve conductivities approaching those of bulk metals. Higher mass loadings or solubilities of the metal nanoparticles are desired in these ink systems, in order to increase ink viscosities and deposit thicker lines for improved device performance.

This study examined the incorporation of multiple ligands onto gold nanoparticles in an effort to increase solubility. Compatibility with plastics is crucial for large-area electronics, so the sintering temperatures of dual-ligand particles were also examined. Nanoparticle solvation was qualitatively assessed through small angle x-ray scattering (SAXS) measurements, while solubility was quantitatively probed through mass-loading drying tests. Both solubility and sintering temperature of dual-ligand nanoparticles were found to be weighted averages of the values for single-ligand particles. Additionally, a trend of increasing solubility with increasing ligand length was found for single-ligand nanoparticle systems.

Acknowledgments

I express my sincere gratitude towards my labmate, Steve Volkman, whose flowing enthusiasm and boundless curiosity have made lab and the office much more enjoyable. Steve was a tremendous help in guiding the methods of my project, as well as its direction when I hit roadblocks, and our detailed discussions of the materials science and chemistry behind my project were invaluable. I am also grateful to Alejandro de la Fuente Vornbrock for helping me understand printed electronics and the need for materials improvement, which lays the motivation for my work. I want to greatly thank Ruth Gjerde, who has always been so kind, supportive, and helpful in addressing any hurdles with the department.

The graduate students in the group helped me acclimate to the research environment and served as role models in academic work, working to thoroughly understand the theoretical and experimental aspects of their research. I thank Tim Bakhishev for his tips on getting my synthesis going, and his discussions of new printable materials. I'd also like to thank Dan Soltman for providing helpful discussions of fluid dynamics, as well as general science findings useful for my project. Shong Yin was extremely supportive with his expertise in lab techniques and our lab space, as well as his insight of materials science and the electrical engineering research landscape. Additionally, these graduate students helped guide me and provided amazing feedback in the strenuous process of applying to graduate school and fellowships.

I'd also like to sincerely thank my advisor, Prof. Vivek Subramanian, for taking me as a Master's student and providing guidance through the tough times of my project. I look up to his extremely solid understanding of device physics and manufacture, and his ability to clearly identify and adapt to the important aspects in science and engineering research.

Finally, I am extremely grateful to my parents, Wei and Yi-Xin, for their love and support through all the years. They frequently went out of their way to help make my life as a student more enjoyable.

Table of Contents

1 Introduction

Printed electronics can help serve the growing need for electronics in today's society. By extending production to large-area and high-throughput reel-to-reel processing, printed electronics offers the capability of producing very low-cost devices, including flexible displays and disposable products like batteries and RFID tags. A printed production process can eliminate the need for costly lithography and vacuum-based deposition steps. Additionally, printing is an additive fabrication process, which minimizes waste by only depositing material as needed.

These benefits for device manufacture apply to several existing printing technologies, including inkjet, gravure, flexography, and screen. However, a common need will be to connect components in printed circuits through the formation of conductive traces. Metal nanoparticles can be incorporated into inks to form conductive lines through these printing technologies. Nanoscale particles provide the added benefit of lowered sintering temperatures compared to flake-based or organometallic inks, yet still provide conductivities comparable to those of bulk metals. Ink properties such as viscosity and surface tension vary according to the printing technology, but a common need is for increased mass loading.

1.1 Motivation – Increased Mass Loading Inks

Inks with increased metal loading allow the printing of thicker, more conformal layers. This enables the formation of lines with sufficiently low resistance, eliminating the need to print multiple passes[1]. Printing multiple passes is not only a costly step timewise, but more importantly, results in worsened roughness and line height variation. If dielectric polymers are used in a printed device, it is crucial to minimize this conductor roughness. Dielectrics are prone to pin-holes and poorly cover ridges and valleys, and addressing this requires additional printing passes or optimization of film reflow[2]. The use of high mass loading inks addresses this, by producing conductive lines with less roughness through single-pass printing. In turn, this permits the use of thinner dielectrics films, creating devices with improved operation

speeds. Finally, the increased solids content commonly leads to higher ink viscosities, which may be important, especially in printing techniques such as gravure printing, which typically require higher viscosity inks to maintain pattern fidelity.

The standard ink used in the Subramanian group is a single-ligand gold nanoparticle solution at 15% mass in α-terpineol. The mass loading could actually be taken higher, but this recipe was well studied and provided a known viscosity and other solvent characteristics suitable to for inkjet printing. The goal of using multiple alkanethiol ligands is to increase the solubility or maximum mass loading, possibly through the creation of greater surfactant surface area, which will increase interaction and solvation with the nonpolar solvent molecules. Along with increased solubility, a decreased sintering temperature for compatibility with plastic substrates is also desired. Thus the use of two ligands to encapsulate gold nanoparticles would ideally increase their solubility while lowering the sintering temperature.

1.2 Background – Colloidal Gold

Gold colloids have been formed for thousands of years, appearing first around the 5th century B.C. in Egypt and China[3]. Their uses ranged from coloring ceramics and glass to eventually, medical drinks in the 17th century. In 1857, Michael Faraday produced a landmark work on synthesis of colloidal metals and their characterization through optical experiments[4]. Faraday prepared a gold colloid through a 2-phase synthesis, with an aqueous solution of a gold salt – sodium tetrachloroaurate ($NaAuCl_4$) being reduced by phosphorus in carbon disulfide (CS_2), a nonpolar solvent. The reduction step rapidly changed the color of the aqueous salt solution from yellow to a deep ruby, and Faraday found the resulting colloidal gold was too small to be observed in any microscope available. Nearly 100 years later, Turkevich utilized electron microscopy[5] to show that Faraday's synthesis resulted in gold particles with a mean diameter of 7±2nm. However, these nanoparticles solutions were not stable, and given time, particles would begin to flocculate, irreversibly aggregating with themselves through attractive van der Waals forces.

1.3 Encapsulated Gold Nanoparticle Synthesis

In order to stabilize the nanoparticles, Brust utilized a protective layer of alkanethiols ($C_nH_{2n+1}SH$). The Brust synthesis, also a 2-phase reduction reaction, was published in 1994 and has made a tremendous impact by providing a facile synthesis of gold nanoparticles that are stable against oxidation and flocculation[6]. The reaction first utilizes a phase-transfer reagent, tetraoctylammonium bromide, to transfer the aqueous gold tetracholoroaurate ($AuCl_4$), to the organic phase, toluene. Next, the gold is reduced by sodium borohydride ($NaBH_4$) in the presence of dodecanethiol ($C_{12}H_{25}SH$), and gold nanoparticles are formed with the thiol ligand strongly binding to the gold surface. The two steps in synthesis are described by the following chemical reactions:

1) $m AuCl_4^-{}_{(aq)} + m N(C_8H_{17})_4^+{}_{(toluene)} \rightarrow m[N(C_8H_{17})_4^+ AuCl_4^-]_{(toluene)}$

2) $m[N(C_8H_{17})_4^+ AuCl_4^-]_{(toluene)} + nC_{12}H_{25}SH_{(toluene)} + 3me^-_{(aq)} \rightarrow$

$$4mCl^-_{(aq)} + (Au_m)C_{12}H_{25}SH_{(n-x)(toluene)} + xC_{12}H_{25}SH_{(toluene)} + mN(C_8H_{17})_4^+{}_{(toluene;aq)}$$

The particles are collected by removing the organic phase with a rotary evaporator, and then washing on a frit filter with ethanol and acetone. To produce the end product of a relatively monodisperse, air-stable powder, several washing techniques exist. Murray's method removes excess thiol with ethanol and excess transfer reagent with acetone[7], while Brust's cleaning method relies solely on an ethanol wash, after suspending the particles at -18°C for 4 hours. In this group, gold nanoparticles prepared by Murray's wash have been used extensively for printable inks. For this study, the dodecanethiol encapsulant was replaced with other alkanethiols, with carbon chain length n = 4, 6, 8, and 12, as well as mixtures of thiols of n=6 and 8, and n = 8 and 12. The alkanethiol names in this report will be used interchangeably with C*n*: (butanethiol – C_4, hexanethiol – C_6, octanethiol – C_8, dodecanethiol – C_{12}). The Brust synthesis is not limited to alkanethiol encapsulation. Various nanoparticle encapsulants, including mercaptophenols and alkylamines, can be attached during the gold reduction step[8], as well as afterwards through place exchange reactions[9].

1.4 Characterization Techniques

In order to characterize nanoparticle size, transmission electron microscopy (TEM) was used[5,7]. The gold cores are imaged, but the organic ligands are transparent to the electron beam. Nonetheless, TEM images give an important measure of the nanoparticles' core size distribution as well as their shape. The method of sizing each particle in a TEM image dates back to Turkevich's 1951 study on size distributions of colloidal gold, but only a fraction of an entire sample can be analyzed. Care must be taken to examine a broad cross-section of a sample to ensure that a representative size distribution is tabulated.

While TEM offers a view of the metal nanoparticle core, the actual arrangement of organic surfactants on the gold nanoparticles can be probed by scanning tunneling microscopy, as shown in Figure 1. This technique is important firstly for discerning whether different surfactants are actually adhering to the nanoparticles. It may be the case that two ligands employed in a nanoparticle synthesis end up creating two kinds of nanoparticles, each with only one ligand. This would result in vastly different solvation properties, and sintering behavior might be expected to occur in a step-wise manner with temperature.

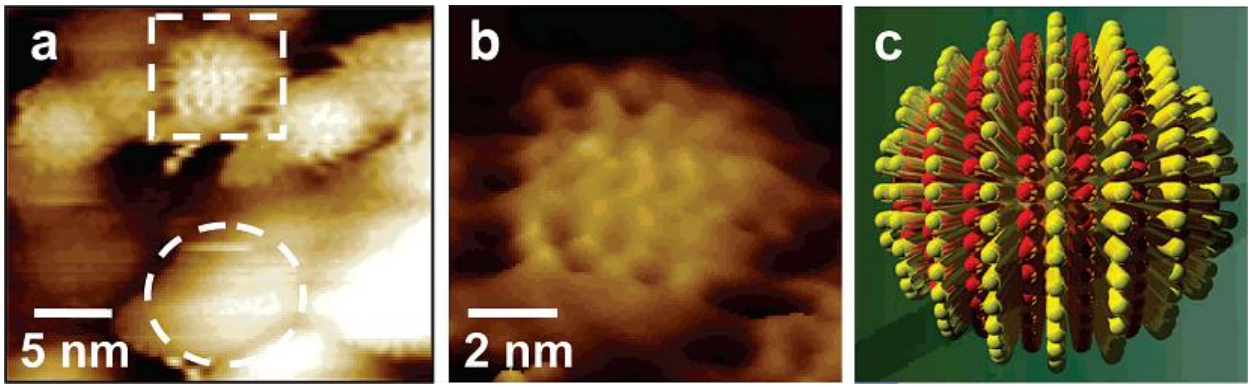

Figure 1 – Scanning tunneling microscope images of dual-ligand gold nanoparticles. Ref. [10] (a) STM image of gold nanoparticles with C_8 and MPA ligands (b) close-up of square in (a). (c) 3D schematic of ligand domains.

In the case that STM determines distinct ligands do exist in the encapsulating layer, it is useful to image their actual arrangement. This helps develop the understanding behind mixing in a solvent, as well as the energetics of ligand removal for sintering. One study of nanoparticles with multiple ligand types found that the varying interfacial free energies

between the solvent and the ligand ends result in an organization of the ligands into ordered domains, which is actually a thermodynamically more stable arrangement than random placement[11]. Centrone studied a system of gold nanoparticles with octanethiol (C_8) and mercaptopropionic acid (MPA), and showed the rearrangement is indeed preferred through surface energy simulations of various arrayed domains.

To ensure the preparation of saturated solutions and properly assess the mass loading, small angle x-ray scattering (SAXS) measurements were used, determining the solvation characteristics[12,13]of solutions, as well as providing additional estimates on nanoparticle size. Solvation analysis is crucial for the later determination of mass loading, by examining the solution for the presence of agglomerates or aggregated nanoparticles. These aggregates can be present in a supersaturated solution, and present an undesired contribution that would incorrectly push the measured solubility to higher values. Observing the SAXS data for samples before and after the preparation step of centrifugation will determine its efficacy in producing a truly saturated solution. The use of SAXS for superlattice size determination was demonstrated by Korgel, who found an effective "soft sphere" diameter for dodecanethiol-encapsulated silver nanoparticles, which is less than the full diameter as predicted by metal diameter plus ligand length[14].

To obtain a SAXS measurement, a monochromatic x-ray source is sent through a sample, and the elastically scattered signal is collected at very small angles, between 0.1 and 10 degrees, as shown in Figure 2. The radiation scatters off of the particles at varying angles Θ, characterized by the scattering vector, $q=4\pi \sin(\Theta)/\lambda$, where λ is the wavelength of the radiation. The intensity is given by $I(q) = c\int_0^\infty n(r)f(qr)S(qr)dr$, where c is a normalization constant, n(r) is the size distribution of the scattering particles, f(qr) is the form factor, and S(qr) is the structure factor. A detailed experiment with dilution measurements can yield values for f(qr), allowing the structure factor and size distribution to be calculated.

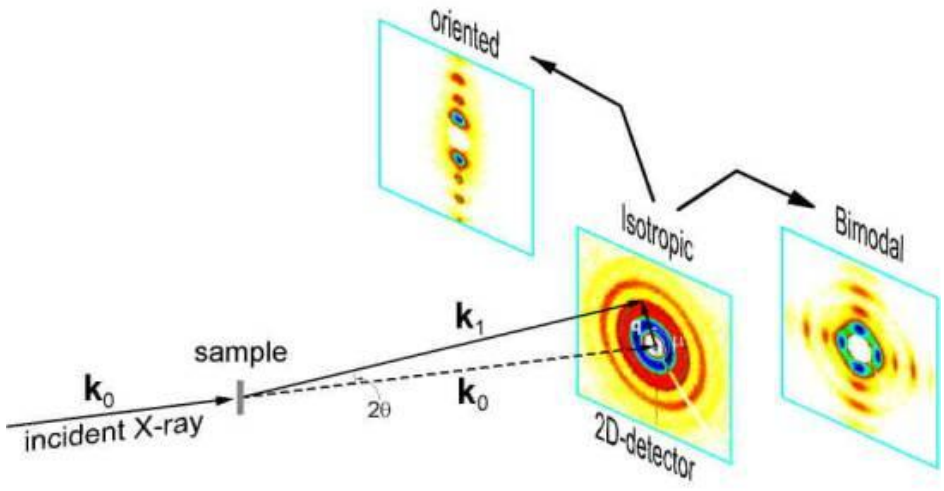

Figure 2 – Small-angle X-ray scattering schematic. Ref. [15] In a solution-based sample, the resulting intensity profile is isotropic, while fixed solid samples may produce asymmetric profiles.

In this study, finding a size distribution is not needed, but qualitative assessment of the SAXS intensities is highly needed to determine the solvation state and presence of superstructure, indicating supersaturation. Above the solubility limit of a solution, further molecules (or in this case, nanoparticles) cannot be individually solvated, and they stay crystallized (agglomerated, forming a nanoparticle crystal or superlattice). These agglomerates should precipitate to the bottom of the solution container, leaving only a saturated solution in the supernatant, but the kinetics of the system may be so slow as to allow the aggregates to remain suspended metastably. The lattices that these metastable aggregates form show up strongly in the SAXS spectra, owing to Bragg diffraction at the superlattice d-spacings. Therefore, any strong peaks in the SAXS spectra, in contrast to a broader signal by single-particle scatterers in solution, will indicate the presence of agglomerates.

Once a saturated nanoparticle solution can be properly prepared, the solubility or loading of nanoparticles can be measured. Nanoparticle solubility is conventionally determined through optical absorption experiments, by examining the decay of the plasmon resonance wavelength. For gold nanoparticles in our size range of 1-5nm, there is a plasmon resonance around 520nm. By measuring these intensities from known dilute concentrations of nanoparticles, a molar extinction coefficient can be calculated, which can be used to determine the concentrations of more saturated solutions[16]. However, the application of this method to

very concentrated solutions is difficult due to high opacity. For this study, the solubility is measured through simple mass loading experiments. By measuring the mass of a nanoparticle solution before and after driving off the solvent, one can determine the dissolved solids content, or the solubility of the nanoparticles.

1.5 Solubility

Solubility of gold nanoparticles has been well-studied in polar solvents[17], but more investigations are being conducted in organic solvents[11,18]. A general rule for solvation is "like dissolves like"; that is, a species is more likely to dissolve well in a solvent of similar polarity. The exposed tails of the gold nanoparticles are the non-polar alkane chains of the alkanethiols, which make them readily dispersed in non-polar solvents such as hexane and toluene. Despite the polar end groups of α-terpineol, nonpolar groups span the majority of the solvent molecule, providing sufficient interaction to solvate alkanethiols. Figure 3 shows the chemical structures of the non-polar molecules used in this study[19].

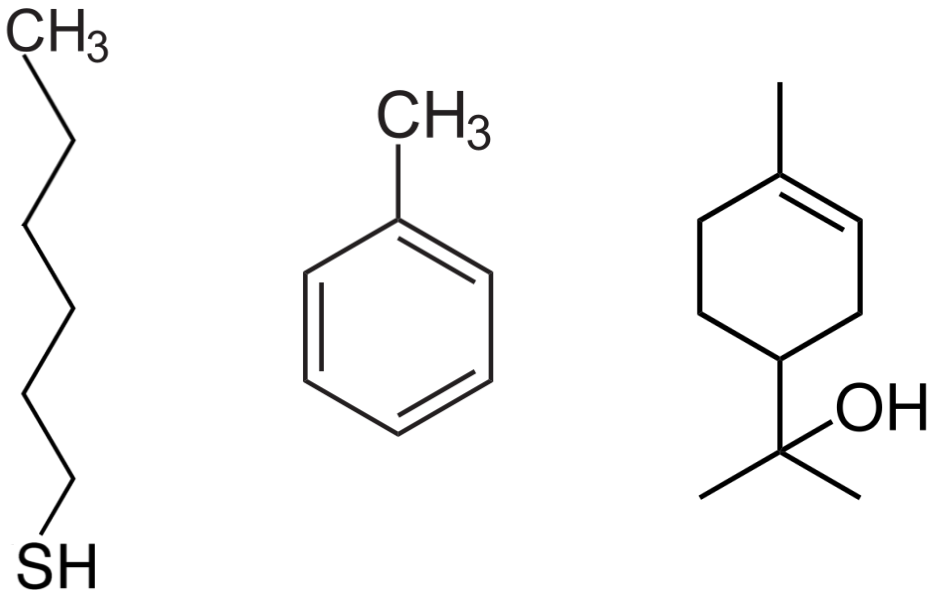

a) Hexanethiol b) Toluene c) α-Terpineol

Figure 3 – Chemical structure of non-polar molecules. Ligand (hexanethiol) and solvents (toluene and α-terpineol). Ref[19]

Toluene is a desirable solvent for study due to its common use, as well as its simple nonpolar structure. However, a different solvent, α-terpineol has a wide application in inks and also represents a good system for study despite its more complex structure, which makes the understanding of molecular solvation physics more difficult. The high viscosity and boiling point of α-terpineol make it an invaluable carrier ink for nanoparticles and the solvent has long been in use by the Subramanian group as well as other printable electronics researchers.

While molecular solvation is a condition of thermodynamic equilibrium, kinetics nonetheless plays a large role in the stability of colloidal solutions. The interplay between electrostatic repulsion and van der Waals attraction of particles forms the basis of Derjaguin Landau Verwey and Overbeek (DLVO) theory. Strong electrostatic repulsion can dominate the van der Waals forces, providing for colloidal stability by keeping particles far apart and preventing flocculation. If the attractive van der Waals forces play a larger role, or if the electrostatic attraction is screened more by an electrolyte, a local minimum can form for stable solvation, while an energy barrier prevents further attraction and subsequent flocculation[20].

1.6 Low-Temperature Sintering of Nanoparticles

In order to form conductive traces, the gold nanoparticles must first eliminate their organic encapsulant and then sinter together to form a continuous low-resistance material. Huang suggested that this occurs in a 2-step process, where the alkanethiol ligands sublimate while heating, and the remaining gold nanoparticles melt and fuse together to form gold films[21]. Due to the nanoscale geometries, the gold particles exhibit vastly reduced melting temperatures from the bulk temperature of 1064 °C. Pawlow[22] and Buffat[23] showed the amount of melting point depression for a sphere is inversely proportional to the particle radius. For compatibility with plastics, nanoparticle sintering temperatures of under 200 °C are desired. Gold nanoparticles of less than 5nm diameter can achieve these low melting temperatures, but the energetics of encapsulant molecules must also be considered. This examination of quantities including the enthalpy of mixing, enthalpy of ligand disordering, and entropy of ligand disordering is important, but outside the scope of this investigation.

2 Experimental

Gold nanoparticles were first synthesized in a two-phase solution process. Particle sizes were analyzed by TEM. Solubility behavior was qualitatively analyzed by small angle x-ray scattering (SAXS), and quantitatively through mass-loading tests. Their solubility was initially analyzed in toluene, but the mass loading was too high to discern differences between particles with different surfactants. The solvent was changed to alpha-terpineol, a common ink basis, and solubility trends were observed while varying the nanoparticle surfactants. Finally, sintering tests were conducted to determine thiol sublimation temperatures, demarcating a minimum for conductive sintering.

2.1 Materials

The chemicals used in the synthesis were gold(III) chloride hydrate (99.999%), tetraoctylammonium bromide (98%), sodium borohydride (98.5%), 1-butanethiol (99%), 1-hexanethiol (95%), 1-octanethiol (98.5%), and 1-dodecanethiol (98%). Each chemical was purchased from Sigma-Aldrich. The solvents used were acetone, ethanol, α-terpineol, and toluene. HPLC grade acetone and toluene were acquired from Fisher Scientific, while ethanol (200 proof) was from Rossville, and α-terpineol (tech. grade, >90%) was from Sigma-Aldrich.

2.2 Synthesis

Alkanethiol-encapsulated gold nanoparticles were synthesized following Murray's method[7], which follows the original Brust two-phase synthesis with a differing wash step. A standard recipe (described below) for hexanethiol-encapsulated gold nanoparticles developed by the group's Daniel Huang was used, and modified by replacing with other alkanethiols. Aside from hexanethiol (carbon chain length n=6), other alkanethiols were used, including those with n = 4, 8, and 12, as well as mixtures of thiols with n=6 and 8, and n = 8 and 12.

First, 12.10g tetraoctylammonium bromide was dissolved in 645mL toluene. 2.5g gold chloride hydrate was dissolved in 200mL deionized water, and transferred to the stirring toluene solution. The organic phase becomes orange-brown when the gold has transferred, and is separated from the aqueous phase. Next, 4.152mL hexanethiol was added (in the case of a 4:1 thiol to gold ratio), and the solution was stirred for 15 minutes. If enough thiol is added (greater than 2:1 thiol to gold ratio), the solution color changes to pale yellow or a cloudy white as the thiols coordinate with gold atoms. Finally, 3.065g sodium borohydride is added to 200mL of deionized water, and this reduction solution is added to the organic solution over a 15-second period. The solution turns dark brown and is left to fully reduce for 3 hours. All synthesis steps occur at room temperature.

To wash the particles, the aqueous phase was discarded, and the organic solvent was removed in a rotary evaporator. The evaporating flask was heated in a water bath at 32.5 °C to accelerate evaporation, while still being a low enough temperature to prevent gold cluster decomposition and surfactant removal. The dried particles were re-suspended in 242mL ethanol, and sonicated as needed to completely remove the products. Finally, the suspended particles were collected on a glass filtration frit, and washed with 645mL ethanol and 1210mL acetone. The remaining gold nanoparticles were left in air to dry for 20 minutes, and collected from the frit filter with a spatula. Particles were stored in a freezer (-20 °C) in air.

2.3 Transmission Electron Microscopy (TEM)

Transmission electron microscope images of the gold nanoparticles were taken using a JEOL 2011 operating at 200keV. TEM grids were prepared by solubilizing samples in toluene, and dropping onto 200-mesh carbon-coated (Type B) copper grids from Ted Pella. Digital images were captured using a TVIPS FastScan F114T CCD and EM-MENU 4 software interface, and nanoparticle sizes were measured with GIMP software.

2.4 Small Angle X-ray Scattering (SAXS)

Small angle x-ray scattering data was collected from beamline 1-4 at the Stanford Synchrotron Radiation Laboratory (SSRL) in Menlo Park, CA. The bending magnet for this synchrotron source was operated at 8.333keV, producing monochromatic radiation of wavelength $\lambda = 1.488$ Å. Scattered photons were collected with a gas-filled detector, and background scattering was accounted for by taking a dark current exposure with the x-ray beam off. Scattering by the Kapton walls, as well as the toluene and α-terpineol solvents was accounted for by subtracting the contribution of blank cells with solvent only. Absorption by the sample was accounted for by recording beam intensities from ionization chambers placed in front of and behind the sample. Angular calibration was performed using a silver behanate reference sample. Data was then integrated using FIT2D analysis software.

2.5 Characterization of Solubility – Mass Loading

Saturated solutions were prepared by loading a high mass percentage (40-80%) of gold into toluene and α-terpineol solvents in polypropylene microcentrifuge tubes. The tubes were then vortex-mixed and sonicated, twice in alternation, to assure full dissolution of the nanoparticle powder into the solvent. To induce settling and be left with a maximally stable concentration of nanoparticles in solution, samples were centrifuged for 15 minutes at 14g (13krpm) on a VWR Galaxy 14D centrifuge. This was found to be sufficient through the comparison of samples centrifuged for times up to 2 hours, and those at lower accelerations down to 8.1g.

To measure the mass loading, a vessel's mass was taken while empty, then with solution, and finally after solvent drying, leaving only the gold nanoparticles. The supernatant was transferred with a micropipette from a centrifuged solution to ensure an accurate saturated solution sample was extracted. There is assumed to be no evaporation in the time between solution deposition and measurement. Due to toluene's high volatility, a fresh microcentrifuge tube was used as the drying vessel, because it offered a quickly closeable cap to prevent evaporation. Complete drying of the solvent occurred at room temperature over

the span of several hours, and was checked overnight for further evaporation. The high boiling point of α-terpineol (217 °C) allowed and required the use of an open vessel – a glass slide, which increased vapor transport and facilitated the use of a hot plate to accelerate drying. The use of tech. grade (90%) α-terpineol allowed the room temperature use of the solvent, since the melting point of pure α-terpineol is 39 °C. The remainder of the solvent is the γ isomer, assumed to play a minimal role in solvation. Drying these samples at 100 °C took between 5 and 15 minutes.

2.6 Characterization of Sintering Temperature

The thiol sublimation or blow-off temperature was determined for the samples, serving as a guideline for the electrical sintering temperature. The sublimation temperatures form a lower bound for the sintering temperatures, as ligands must be removed before gold particles can coalesce and form a continuous conductor[21]. The hot plate was slowly ramped, at a rate of 4K/min, and the sample was closely monitored for color change. The thiol sublimation temperature was recorded as the point of discernable color change in the nanoparticle film from black to gold.

3 Results and Discussion

3.1 Nanoparticle Sizes Determined via TEM

Nanoparticles were grown at thiol-gold mole ratios of 4:1 or 8:1, giving fairly tight size distributions. A summary of synthesis results, grouped by thiol encapsulant(s) and thiol-gold ratio is given in Table 1. Sizes were slightly bigger than expected, when comparing with the 1.5nm diameter particles synthesized by Huang and Murray under similar conditions. Though a larger thiol-gold ratio is expected to decrease size (Huang's 1:12 ratio produced 5nm particles), increasing the thiol-gold ratio to 8:1 actually increased particle sizes in most cases. Since a thiol-gold ratio of 4:1 is already deep in the saturated regime, the increased nanoparticle size may be a result of the large excess in thiols inhibiting their own diffusion, while the reduction process continues and gold cores nucleate.

Table 1. Diameter Sizes of Synthesized Nanoparticles

Thiols (ratio)	Thiol:Au	Size (nm)	Sample #	StDev (nm)
C_6	4	2.6	D	0.62
C_6	8	2.72	U	0.59
C_8	4	2.66	A	0.83
C_8	8	2.16	B	0.61
C_6/C_8 (1:10)	4	2.37	G	0.47
C_6/C_8 (1:1)	4	2.04	E	0.47
C_6/C_8 (10:1)	4	2.49	F	0.97
C_6/C_8 (10:1)	4	2.37	W	0.59
C_6/C_8 (10:1)	8	2.92	H	0.78
C_6/C_8 (10:1)	8	3.96	V	1.36
C_8/C_{12} (5:1)	4	2.32	C	0.74

Nanoparticles synthesized were all in the 2.7nm range, with the exception of sample V, with a mean of 3.96nm and wider spread in sizes. However, all particles are well under 4nm, and the sizes are close enough together that size effects can be largely ignored in the discussion

of solubility. A representative TEM image is shown Figure 4 for sample H at 300kX magnification. Figure 5 shows sample W, a C6/C8 sample at the standard thiol-gold ratio of 4:1. A high magnification (800kX) image of sample V is shown in Figure 6, where gold lattice fringes are visible.

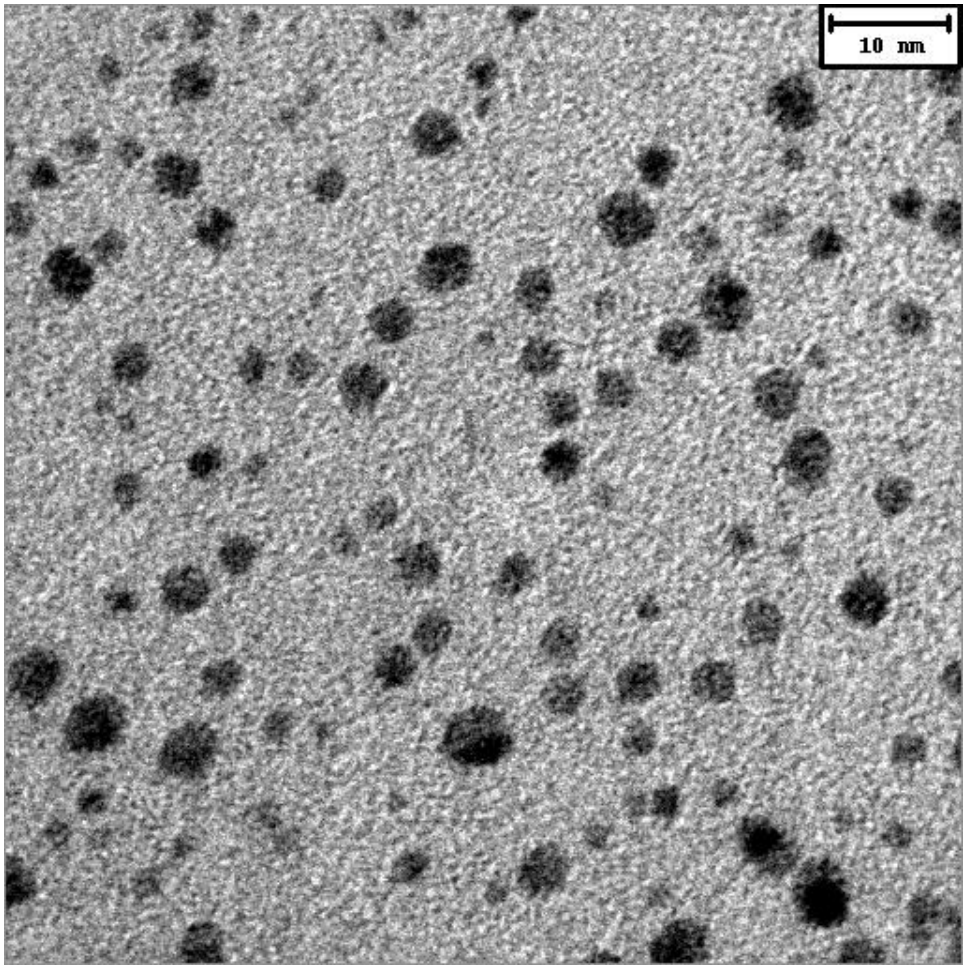

Figure 4 – TEM image of sample H (C_6/C_8 in 10:1 ratio) at 300kX magnification. Average diameter: 2.92nm.

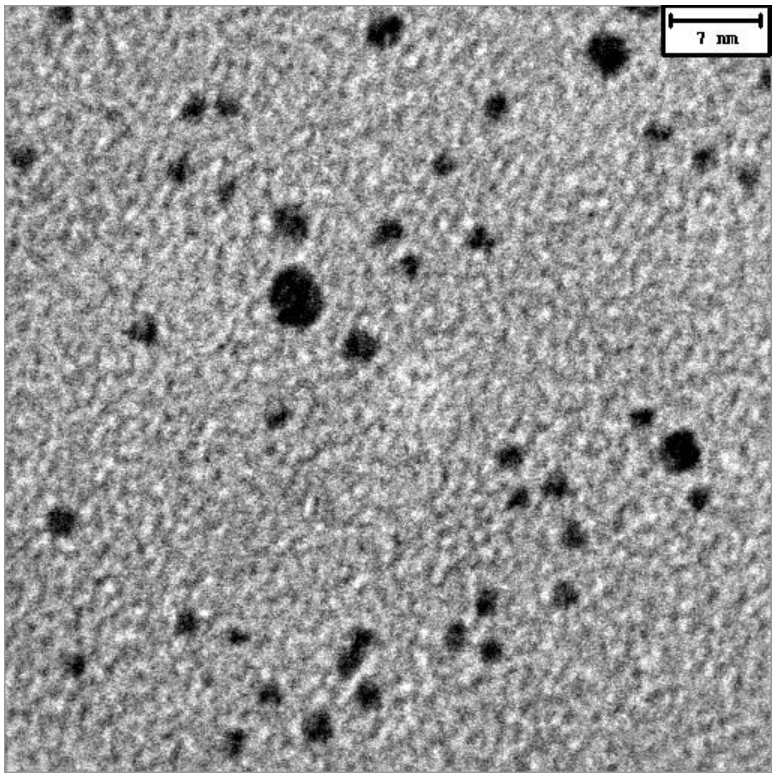

Figure 5 – TEM image of sample W (C_6/C_8 in 10:1 ratio) at 400kX magnification. Average diameter: 2.72nm.

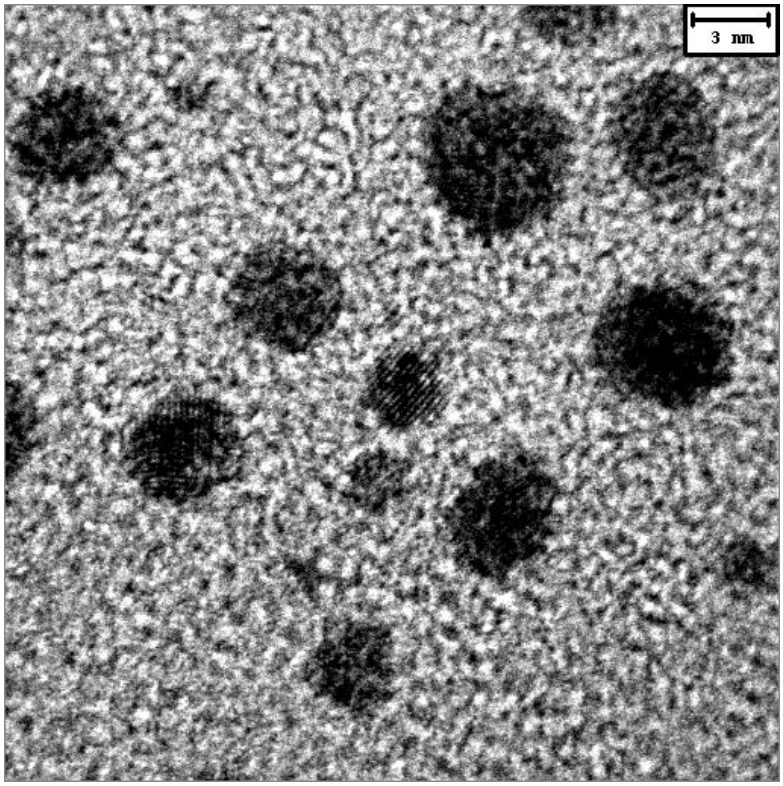

Figure 6 – TEM image of sample V (C_6/C_8 in 10:1 ratio) at 800kX magnification. Average diameter: 3.96nm.

Several samples used in the solubility study were not imaged under TEM, and were assumed to have similar sizes, drawing from the studies of prior syntheses. These nanoparticles were all grown at a thiol-gold ratio of 4:1, and comprise samples K (butanethiol, C_4), X (octanethiol, C_8), Y (dodecanethiol, C_{12}), and Z (octanethiol/dodecanethiol, C_8/C_{12} in a 10:1 ratio). From the size results in Table 1 as well as those presented by Huang, there is little correlation in the saturated regime of thiol-gold ratio of 4:1, between encapsulant length and nanoparticle size. Thus, the nanoparticles encapsulated by butanethiol and dodecanethiol can be assumed to have a similar size (around 2.7nm) as the hexanethiol and octanethiol encapsulated particles.

3.2 Solvation Evaluated by SAXS

The observation of important solution characteristics, most notably, supersaturation, was enabled through small angle x-ray scattering measurements. A first set of SAXS data was acquired for toluene-based solutions to evaluate the validity of using SAXS for analyzing solvation. Concentrated solutions of 66% mass percent gold nanoparticles were measured, as well as dilutions by factors of 2, down to $(1/2)^6$ or 1.5625%. The solutions were vortex-mixed for 30 seconds, but were not sonicated or centrifuged. Thus, due to the lack of a sonication step, the characterization results may not represent a complete loading or dissolution of nanoparticles into solution. However, the solution could still have been supersaturated, because there was no centrifugation step to precipitate or crash out nanoparticles. SAXS spectra are shown in Figure 7 through Figure 9, and the intensities for dilutions have been shifted for clarity. The character of SAXS intensities did not change significantly for dilutions less than 8.25% and are not shown.

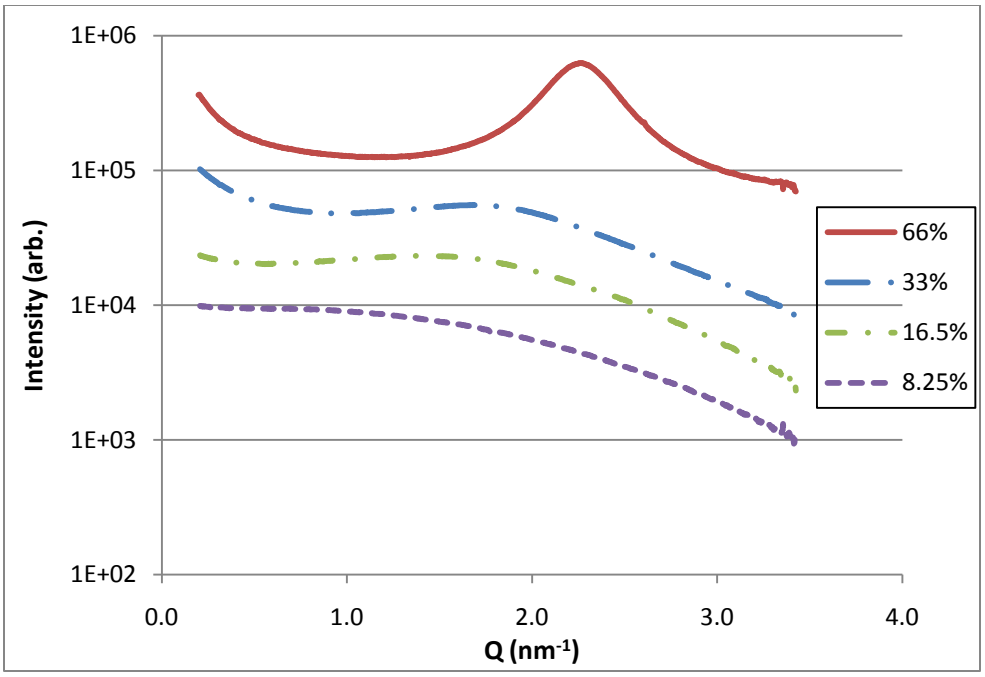

Figure 7 – SAXS plot of sample C (C_8/C_{12}=5) at 4 highest dilutions.

Sample C showed a strong high-Q peak at the maximum concentration, corresponding to presence of a superlattice, suggesting supersaturation of the solution. It is also possible that clusters are solvated in toluene, because there was no sonication step, and these clusters could contribute to superlattice scattering. All toluene samples (C, D, and F) showed similar behavior, with superlattice peaks present at the highest 66% concentration, and disappearing immediately in the next dilution of 33%. Sample C showed a strong peak at Q = 2.264 nm^{-1}, while samples D and F exhibited peaks at Q = 2.136 nm^{-1} and 2.223 nm^{-1}, respectively.

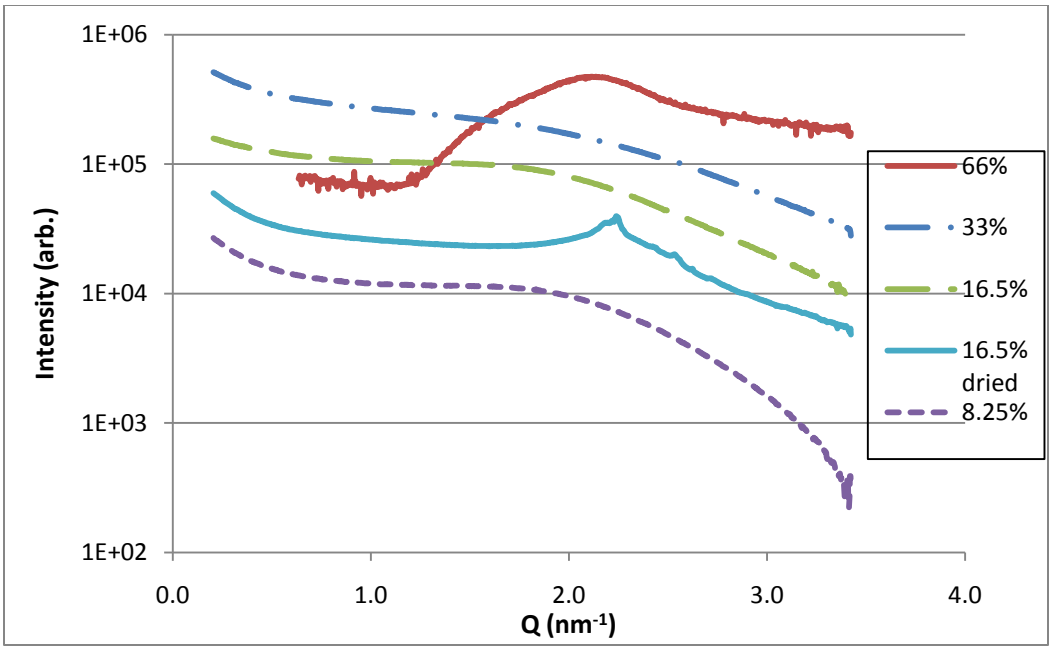

Figure 8 – SAXS plot of sample D (C_6) at highest 4 dilutions and a dried 16.5% dilution.

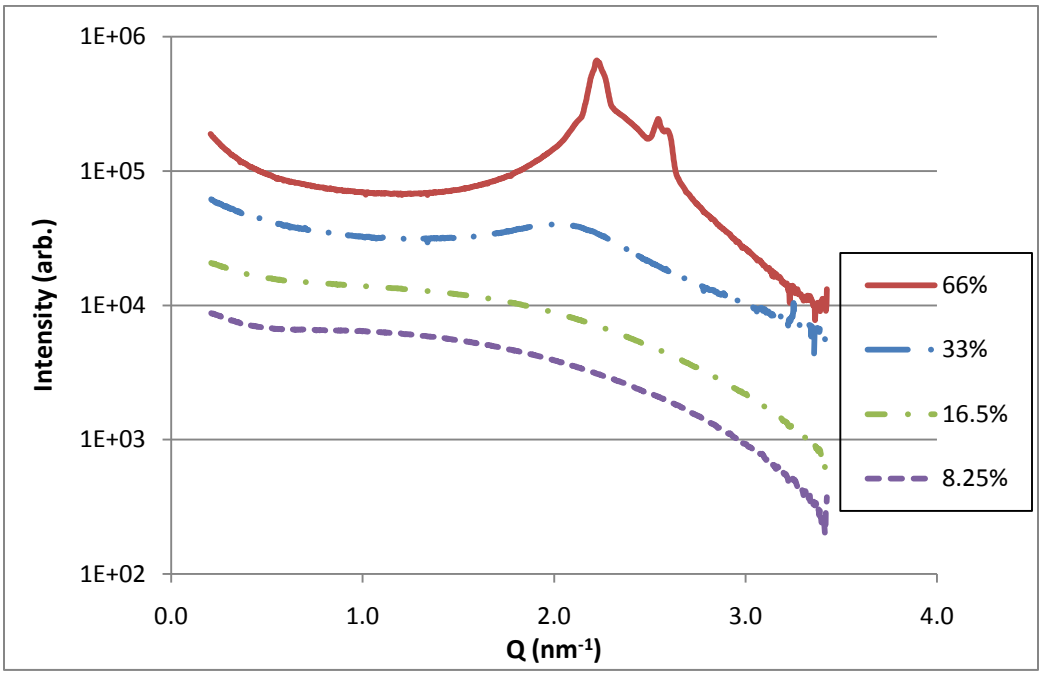

Figure 9 – SAXS plot of sample F (C_6/C_8 = 10) at highest 4 dilutions.

Interestingly, the peak disappears in dilutions of sample D, but reappears for a solution with visible dried particulate, as shown Figure 8. Though the dilution was prepared at 16.5% mass gold nanoparticles, there was an evaporation route for the toluene, and one cannot

determine the true loading of the sample. The peak is sharp due to the adhesion of the dried nanoparticle clusters onto the Kapton side walls, providing for exact preferential scattering directions. It is worth noting that the peak of the dried sample (Q = 2.240 nm^{-1}) aligns well with that of the supersaturated peak (Q = 2.136 nm^{-1}). Both arise from the presence of a superlattice, with the slight difference possibly arising due to a different ordering preference. This may be the result of the Kapton surface, as well as the high concentration of toluene providing a different crystallization environment than the air and acetone environment where the initial cluster was formed.

The Q-values can be analyzed to extract nanoparticle spacing in the superlattice, but values obtained by SAXS tend to underestimate length scales produced by TEM. The Q values correspond to d-spacings for Bragg reflection, following $Q = 2\pi/d$. Assuming the nanoparticles form in a hexagonal closed pack array, as is most common for spherical particles, a relation can be expressed[24] for particle center-to-center spacing α, given by:
$Q_{hk} = 4\pi(h^2+k^2\ hk)^{0.5}/(3^{0.5}\alpha)$ for scattering indices of integer values of *h* and *k*. Assuming the main peak arises from scattering at h,k = 1,0, calculated values of α are shown in Table 2. The value calculated from the TEM diameter utilizes the theoretical chain length for alkanethiols, given by L = 2.5 + 1.27*n* Å, where *n* is the carbon chain length.

Table 2. Values of Particle Center-to-center Spacing from TEM and SAXS

Sample #	Ligand	Q (nm^{-1})	Ligand L (nm)	d_{TEM} (nm)	α_{TEM} (nm)	α_{SAXS} (nm)
C	C_8/C_{12}	2.264	1.774	2.32	4.09	3.20
D	C_6	2.136	1.012	2.60	4.62	3.40
F	C_6/C_8	2.223	1.266	2.49	3.76	3.26

The longest ligand present was assumed to define the interparticle spacing. The center-to-center spacing calculated by the TEM determined size is given by $\alpha_{TEM} = d_{TEM} + L_{ligand}$, assuming full interdigitation, and the long alkanethiol spans the distance between nanoparticle edges. However, the hexanethiol-only sample was assumed to be a hard-sphere, with 2 hexanethiol lengths accounting for the separation. As evident in Table 2, all values calculated from SAXS data were smaller than predicted from TEM data. This may have been due to TEM

imaging biasing towards larger particle sizes, or also ligand lengths varying from the theoretical formula, and finally a manifestation of the "soft shell" behavior described previously[14]. A superlattice length scale was determined by SAXS but was not necessary for the purpose of studying solvation.

Dilutions of 33% and lower show a regime of low-Q scattering, which drops significantly at higher Q. The plot can be fit with Porod's law to determine a size distribution n(r) for particles, but the characteristic radius of nanoparticle scatterers can be estimated as the intersection of the 2 regions. The shift of the curve to lower Q at higher dilutions agrees with previous SAXS studies on colloidal dilutions, corresponding to the increase of interparticle spacings[13]. The shift to lower Q is accompanied by a decrease in scattering intensity, as is expected for dilute solutions. In conclusion, the data provided by the toluene samples successfully showed solvation characteristics, indicating the existence of clusters or superlattices in high concentration samples.

This method was repeated for α-terpineol solutions and used to assess techniques for preparing saturated samples. The solvent was changed from toluene, because the mass loading experiments found toluene to be overly soluble (over 70-80% mass gold loaded), and unsuitable for experimentation. Two concentrations were tested – 40% and 20%, which were vortex-mixed and sonicated during preparation. As with the toluene solutions, SAXS spectra for the α-terpineol solutions showed superlattice peaks at higher concentrations (Figure 10 and Figure 11). After centrifugation, the superlattice peak disappeared from the spectra, indicating the crashing out or precipitation of supersaturated clusters. The loss of peaks in samples U and W signified a successful preparation of a saturated solution, with the maximum concentration of gold nanoparticles driven into solution, and the excess, unsolvated clusters precipitated out.

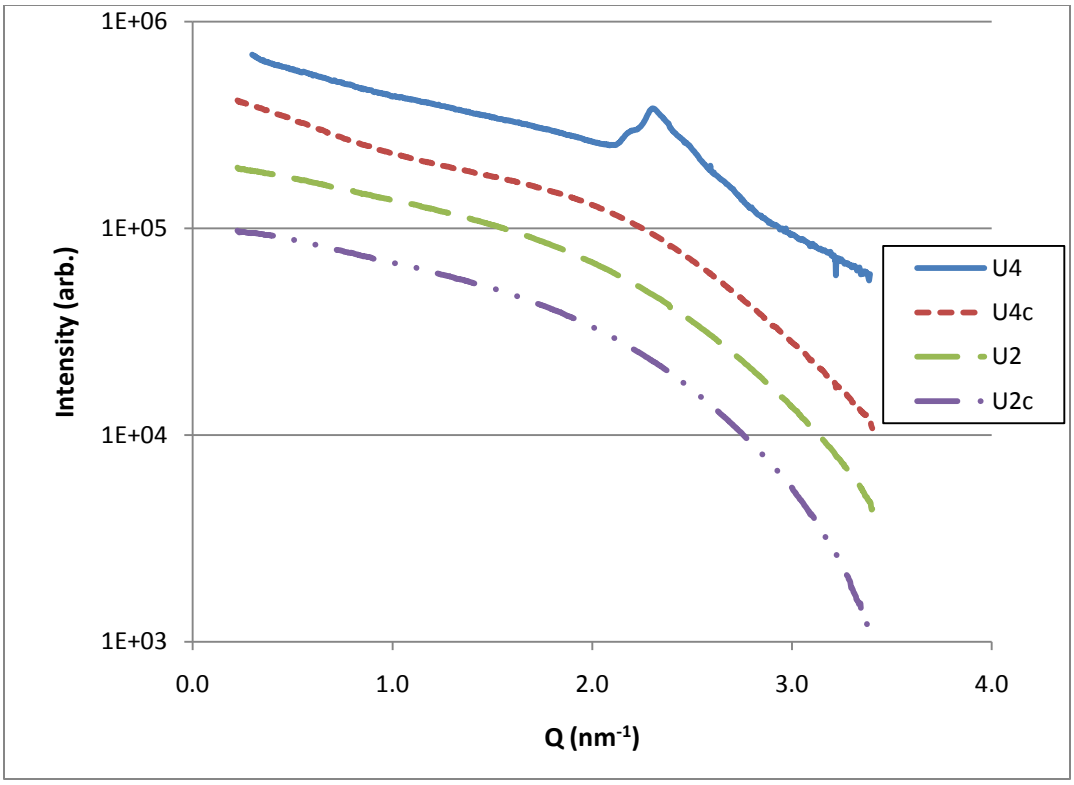

Figure 10 – SAXS plot of sample U for 40% and 20% conc., before and after centrifuge (denoted by 'c')

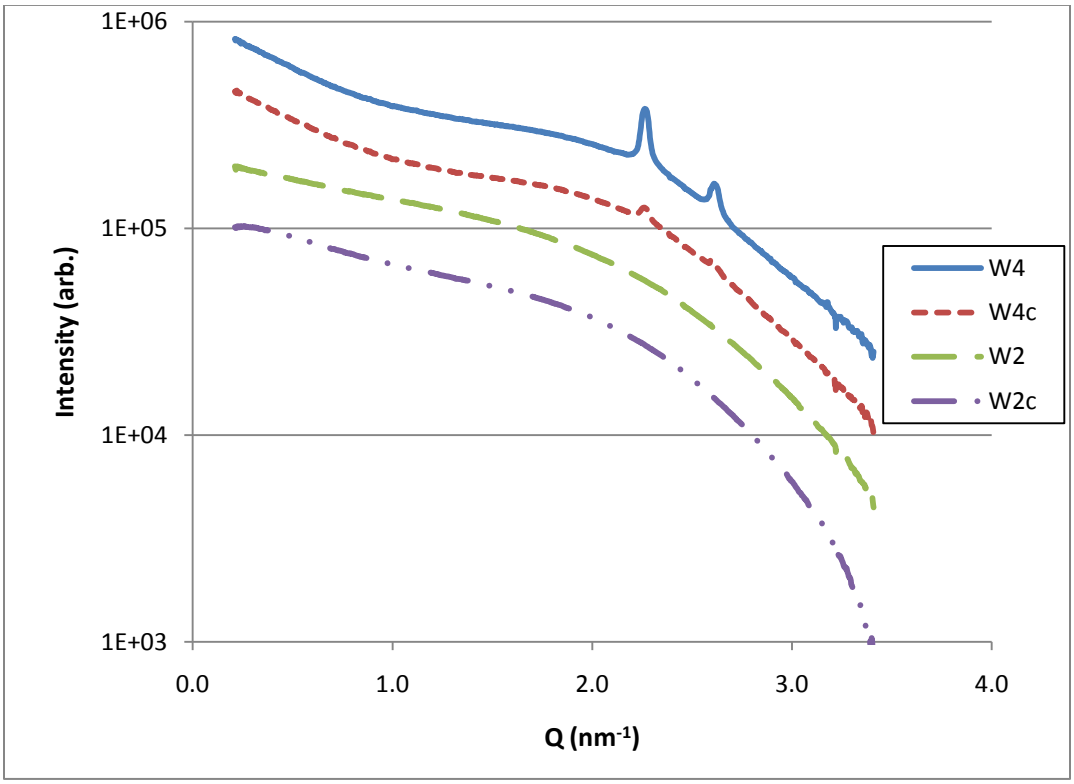

Figure 11 – SAXS plot of sample W for 40% and 20% conc., before and after centrifuge (denoted by 'c')

Sample W (C6/C8=10) shows two interesting observations in Figure 11: 1 – the presence of 2 peaks in the uncentrifuged 40% sample, and 2 – the post-centrifuge 40% sample contains a minor peak at the same Q value corresponding to the superlattice. The presence of the second peak may be the result of a different reflection of the same type of superlattice as the first peak, or perhaps the presence of a different superlattice ordering, which arise from the dual-ligand nanoparticles. The minor peak in the centrifuged sample is a remnant of the supersaturated cluster from an uncentrifuged sample, with the low intensity indicating it is present in a much smaller concentration. This may be due to disturbing the precipitated solution, or perhaps penetrating the supernatant down to the clusters while micropipetting the sample.

Two solutions (samples A and V) did not exhibit any superlattice peaks, even in the uncentrifuged high concentrations (Figure 12 and Figure 13). This can be explained by the high solubility of these particles: sample A was octanethiol-encapsulated, with an average diameter of 2.66nm, while sample V was C6/C8-encapsulated, with an average diameter of 3.96nm. Simply put, these nanoparticles were fully dissolved by the α-terpineol, and no aggregates remained to be observed. Mass loading tests showed the as-prepared concentration of 40% mass both before and after centrifugation, meaning the nanoparticles were fully dissolved in the solutions and did not precipitate. The SAXS spectra behaved just like the low dilutions of other samples, with the scattering shifting towards lower Q.

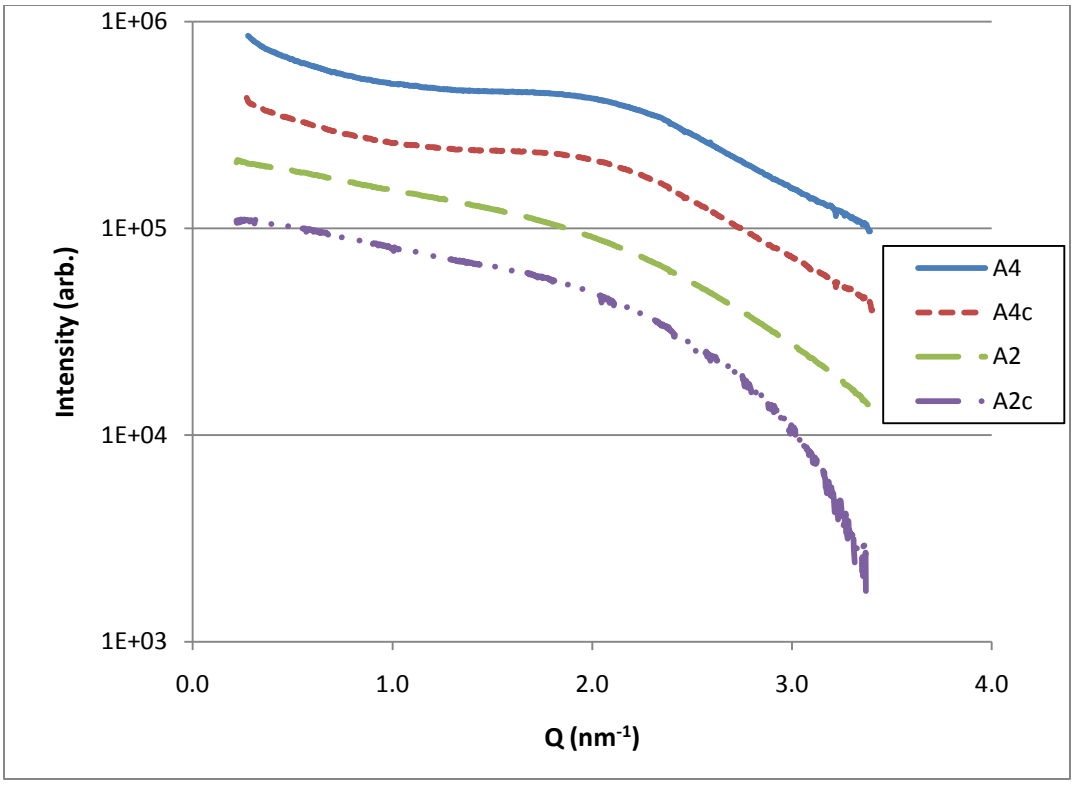

Figure 12 – SAXS plot of sample A (C_8) for 40% and 20% conc., before and after centrifuge (denoted by 'c')

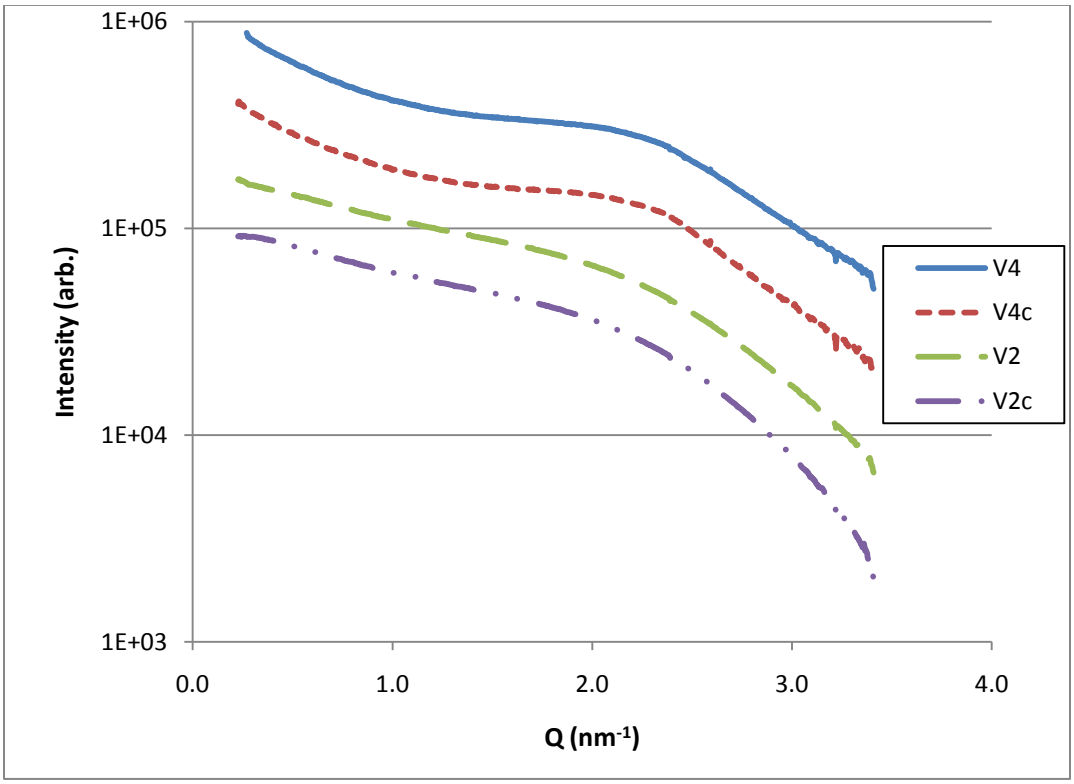

Figure 13 – SAXS plot of sample V (C_6/C_8 = 10) for 40% and 20% conc., before and after centrifuge (denoted by 'c')

In summary, SAXS measurements were quite useful for determining whether a solution was supersaturated, and provided a method to check if centrifugation was successfully producing saturated solutions. The presence of a strong high-Q Bragg peak for all 3 toluene-based nanoparticles showed supersaturation at the initial concentration of 66% mass, which disappeared when diluting to 33%. This is not surprising because the solution was not sonicated (meaning agglomerates stay undissolved), and also not centrifuged (so that clusters are not precipitated to the bottom of the test tube) and remain metastably in solution. The particle center-to-center spacing was extracted from the superstructure peaks in toluene samples, and was found to be smaller than the value prediced from TEM and theoretical ligand length. Next, SAXS spectra of α-terpineol based samples revealed 2 systems to have extraordinary solubility, through the lack of superstructure peak at the highest examined concentration of 40% mass. Finally, in the other 2 systems with initial superstructure, the use of centrifuge to induce precipitation was verified to produce saturated solutions, indicated by the loss of the superstructure peaks after centrifugation.

3.3 Mass Loading Results

Mass loading tests found the nanoparticles to be too soluble in toluene, with solubility differences indiscernible between samples. Specifically, nanoparticles were able to be loaded into toluene solutions to as high a concentration as desired, reaching 70% and 80% mass, even after centrifugation. This meant that characterized solubility values were not exactly determined, but rather a minimum (for the maximum solubility) value was established as the initial concentration in the prepared sample. Furthermore, this presented a challenge for testing more (specifically higher) concentrations, because each solution consumed so much nanoparticle powder. Therefore, the solvent was switched to α-terpineol in order to study a system with lower solubility, and just as importantly, to show a difference between solutions of different nanoparticles. Although α-terpineol is more complex than toluene, confounding the understanding of solvation physics, it nonetheless forms a good system for study due to its wide application in inks for printed materials development.

α-Terpineol provided the desired decrease in solubility and demonstrated that nanoparticles with 2 types of ligands have solubilities that are weighted averages of the solubility of particles with only 1 type of ligand. This can be seen by examining C_6-encapsulated sample U, with a low 21.7% mass solubility, and C_8-encapsulated sample X, with 70% solubility (at minimum). Meanwhile, sample W, a dual ligand system of C_6 and C_8 showed an intermediate solubility of 31.4% gold nanoparticle mass. This is a significant decrease from the octanethiol-only solubility of 70%, which can be attributed to the greater composition of hexanethiol ligands (a 10:1 ratio C_6 to C_8) in sample W. It must be noted that the octanethiol solubility of 70% is only a lower limit, for the mass loading was actually found to be identical to the as-prepared solution. This was the issue for the toluene system, but because differences can be resolved between samples in α-terpineol, the determination of a minimum solubility limit is acceptable.

Table 3. Mass Loading Results in α-Terpineol

Sample #	Thiol	Thiol:Au	Diameter (nm)	Mass Load (%)
K	C_4	4	-	2.8
U	C_6	8	2.72	21.7
W	C_6/C_8 (10:1)	4	2.37	31.4
V	C_6/C_8 (10:1)	8	3.96	*40.7
X	C_8	4	-	*70
A	C_8	4	2.66	*53.5
Z	$C_8/_{12}$ (10:1)	4	-	71.5
Y	C_{12}	4	-	*69.1

* indicates load matches as-prepared solution

The solubility values determined for samples A, V, X, and Y must be taken as lower limits on solubility. Sample V, the other C_6/C_8 mixture shows a minimum of 40.7%, which is higher than the 31.4% of similarly coated particles. The difference may be a size effect, as the sample V particles have a significantly greater (67%) mean size. Bauer's study on silver nanoparticles reported solubility in hexane to increase with the nanoparticle core size[18]. The actual solubility limit of sample V is presumably between 40.7% and the 70+% lower limit values for itself and a C_8-only sample, respectively.

The solubility of the butanethiol (C_4)-encapsulated particles was an abysmally low 2.8%. This may have been due to the instability of the butanethiol encapsulation, and testing the particles 2 weeks after synthesis may have led to ligand loss and particle destabilization. Nonetheless, this data point is taken as valid, and it establishes a chain length dependence for solubility: the longer the ligand chain, the higher the solubility. Therefore, the solubility of dodecanethiol (C_{12})-encapsulated particles is expected to be greater than that of particles with C_8. Because both measurements of C_8 and C_{12} encapsulated particles (samples A, X, and Z) were all just solubility lower limits, we must rely on the trend from C_4 to C_6 and C_6 to C_8 to make this conjecture. For example, the maximum solubility of C_8 is, arbitrarily, in the range of 70-80% and that of C_{12} is higher, from 80-90%. This solubility trend with chain length may be specific to thiol-encapsulated gold nanoparticles in α-terpineol. The Bauer study of thiol-encapsulated silver nanoparticles showed a trend of decreasing solubility with increasing ligand chain length[18]. Although the silver-thiol bond is quite different from that of gold, this result is still a surprising contrast to the current study, because solubility is expected to be most related to the interaction with the ligand chains.

The final data point to consider is the solubility of sample Z, encapsulated by a C_8/C_{12} mixture. The original solution of 81% mass loading was precipitated and left the soluble portion in the supernatant, which revealed the solubility to be 71.5% mass. This figure aligns with the conjecture of increasing solubility with chain length, because there is a greater portion of C_8 than C_{12} (10:1 ratio). Thus the weighted average is closer to the lower solubility of C_8 than it is to that of C_{12}. The solubility was unable to be increased by using dual ligands above the solubilities of single ligand systems, largely in part due to the naturally high solubilities of the octanethiol and dodecanethiol systems. However, the solubilities were found to be an average of that of nanoparticles in single ligand systems, a useful result for the future tuning of nanoparticle ink systems.

3.4 Sintering Temperature Results

Thiol sublimation temperatures of dual ligand systems were also found to be weighted averages of the temperatures for single ligand nanoparticles. Values of sublimation temperatures were similar to those found by Daniel Huang for the smaller 1.5nm particles, as the particles in this study were closer in size to those rather than 5nm particles also studied by Huang. A summary of sublimation results are listed in Table 4.

Table 4. Thiol Sublimation Temperatures

Sample #	Thiol	Thiol:Au	Diameter (nm)	Sublimation T (°C)	Huang T [1.5nm] (°C)	Huang T [5nm] (°C)
K	C_4	4	-	138	127	120
U	C_6	8	2.72	171	169	100
W	C_6/C_8 (10:1)	4	2.37	165	-	-
V	C_6/C_8 (10:1)	8	3.96	160	-	-
X	C_8	4	-	160	168-80	160-72
A	C_8	4	2.66	162	168-80	160-72
Z	C_8/C_{12} (10:1)	4	-	165-70	-	-
Y	C_{12}	4	-	180	190	170-80

Sample W, a C_6/C_8 system, exhibited a sublimation temperature of 171 °C, midway between those of the C_6- and C_8-only systems, at 171 °C and 160 °C, respectively. The butanethiol sample showed a moderately higher sublimation temperature than in Huang's study, but still remains the lowest temperature in this study. Though thiol sublimation temperatures are expected to follow the boiling points of the constituent thiols, the C_6 sample shows a slightly higher temperature than the C_8 samples. This disparity was also observed in the Huang study, and here may be due to the effect of size. Despite the presence of far more C_6 in the C_6/C_8 system, the temperature is not closer to the C_6 sublimation temperature. The range of the temperature differences is quite narrow, but in the case of sample Z, the C_8/C_{12} system, the 165-170 °C sublimation temperature is slightly closer to the 160 °C temperature corresponding to C_8, the dominant ligand. Thus this sample showed a weighted average favoring the dominant ligand component in the case of sublimation temperature as well as solubility.

The study of sublimation temperatures found that dual-ligand systems take an intermediate value between temperatures for single-ligand systems. In sample Z (C8/C12), weighting towards the dominant C8 ligand was observed, while sample Z (C6/C8) did not shot much weighting effect towards the more populous C6 ligand. One criticism is that the range for temperature differences between two single-ligand systems is too narrow for this careful of a comparison. Ideally, the nanoparticles would sinter at the temperature of the ligand with lower sublimation temperature, while getting the benefit of improved solubility from the higher-length ligand. However, this was not the case, as both quantities were averages of values for single-ligand systems. Thus the use of two or more types of ligands creates a tradeoff for fabrication routes, between improved solubility and lower sintering temperature. This interplay could become important for tuning ink systems to specific subtsrates – maximizing the solubility for better printability while keeping the sintering temperature sufficiently below the substrate's glass transition temperature.

4 Conclusion

Dual ligand gold nanoparticles were synthesized, and their sintering temperatures and solubilities in toluene and α-terpineol were examined. This study showed the utility of small angle x-ray scattering in assessing the solvation characteristics of nanoparticle solutions, by identifying the presence of superlattice structure. A centrifugation step is critical for driving any supersaturated nanoparticle clusters to precipitate, and produce a desired saturated solution of nanoparticles. Nanoparticles with two different ligands were found to have intermediate solubilities and sintering temperatures representing a weighted average of values for single-ligand particles.

Although the goal of solubility improvement beyond that of single-ligand systems was not achieved, the tunability of the solubility and sintering temperature by varying ligand composition is an important result. The solubility of gold nanoparticles can be increased by introducing higher-length alkanethiols, but it comes with the tradeoff of higher sintering temperature, an undesirable characteristic for printed electronics. In order to better understand the relationship of thiol-encapsulated nanoparticles with solubility, an investigation on size effects will be crucial. Additionally, a scanning tunneling microscope (STM) investigation may be necessary to observe the actual configuration of different ligands on nanoparticles and whether they form distinct single-ligand nanoparticles. Again, emphasis is placed on determining size effects, because its strong relation to sintering temperature may make the variation of size just as important as ligand composition for the pursuit of higher solubility and lower sintering temperatures. Finally, dual-ligand nanoparticles need to be looked at from a printed inks perspective, to ensure the modified particles can still deliver key metrics such as jettability and low roughness.

5 Works Cited

[1] Redinger, D.; Farshchi, R.; Subramanian, V. An All-Printed Passive Component Technology for Low-Cost RFID. *61st Device Research Conf. (DRC 2003)* Conference Digest, Piscataway, NJ: IEEE Press, **2003**, pp. 187-188.

[2] Molesa, S.; Redinger, D.R.; Huang, D.C.; Subramanian, V. High-quality inkjet-printed multilevel interconnects and inductive components on plastic for ultra-low-cost RFID applications. *Mat. Res. Soc. Symp. Proc*., **2003**, Vol. 769, H8.3.1-H8.3.6

[3] Daniel, M.C.; Astruc, D. Gold Nanoparticles: Assembly, Supramolecular Chemistry, *Chem. Rev.* **2004,** *104,* 293-346.

[4] Faraday, M. Experimental Relations of Gold (and other Metals) to Light. *Philos. Trans.* **1857**, *147*, 145-181.

[5] Turkevitch, J.; Stevenson, P. C.; Hillier, J. Nucleation and Growth Process in the Synthesis of Colloidal Gold. *Discuss. Faraday Soc*. **1951**, *11*, 55-75.

[6] Brust, M.; Walker, M.; Bethell, D.; Schiffrin, D. J.; Whyman, R. J. Synthesis of Thiol-Derivatized Gold Nanoparticles in a Two phase Liquid-Liquid System. *J. Chem. Soc., Chem. Commun.* **1994**, 801-802.

[7] Hostetler, M. J.; Wingate, J. E.; Zhong, C.-J.; Harris, J. E.; Vachet, R. W.; Clark, M. R.; Londono, J. D.; Green, S. J.; Stokes, J. J.; Wignall, G. D.; Glish, G. L.; Porter, M. D.; Evans, N. D.; Murray, R. W. Alkanethiolate Gold Cluster Molecules with Core Diameters from 1.5 to 5.2 nm: Core and Monolayer Properties as a Function of Core Size. *Langmuir* **1998**, *14*, 17-30.

[8] Brust, M.; Fink, J.; Bethell, D.; Schiffrin, D. J.; Kiely, C. J. Synthesis and Reactions of Functionalised Gold Nanoparticles. *J. Chem. Soc., Chem. Commun*. **1995**, 1655-1656.

[9] Templeton, A. C.; Hostetler, M. J.; Kraft, C. T.; Murray, R. W. Reactivity of Monolayer-Protected Gold Cluster Molecules: Steric Effects. *J. Am. Chem. Soc.* **1998**, *120*, 1906-1911.

[10] Jackson A.M.; Hu Y.; Silva P.J.; Stellacci F. From homoligand- to mixed-ligand monolayer-protected metal nanoparticles: A scanning tunneling microscopy investigation. *J. Am. Chem. Soc.* **2006**, 128:11135–11149.

[11] Centrone, A.; Penzo, E.; Sharma, M.; Myerson, J.W.; Jackson, A.M.; Marzari, N.; Stellacci, F. The role of nanostructure in the wetting behavior of mixed-monolayer-protected metal nanoparticles. *Proc. Natl. Acad. Sci. USA.* **2008**, 105, 29, 9886–9891

[12] Huang, E.; Toney, M.F.; Volksen, W.; Mecerreyes, D.; Brock, P.; Kim, H.C.; Hawker, C.J.; Hedrick, J.L.; Lee, V.Y.; Magbitang, T.; Miller, R.D.; Lurio, L.B. Pore size distributions in nanoporous methyl silsesquioxane films as determined by small angle x-ray scattering. *Appl. Phys. Lett.* **2002**, 81,12, 2232-2234.

[13] Ingham, B.; Dickie, S.; Nanjo, H.; Toney, M.F. In situ USAXS measurements of titania colloidal paint films during the drying process. *J. Colloid Interface Sci.* **2009**, 336, 612-615.

[14] Korgel, B.A.; Fullam, S.; Connolly, S.; Fitzmaurice, D. Assembly and self-organization of silver nanocrystal superlattices: ordered "soft spheres". *J. Phys. Chem. B* **1998,** *102,* 8379-8388

[15] Wiesner Group – Small Angle X-Ray Scattering http://people.ccmr.cornell.edu/~uli/pages/saxs.htm Cornell University, **2008**.

[16] Liu X, Atwater M, Wang J, Huo Q. Extinction coefficient of gold nanoparticles with different sizes and different capping ligands. *Colloids Surf B* ***2007*** 58:3–7.

[17] Mulvaney P. Metal Nanoparticles: Double Layers, Optical Properties, and Electrochemistry. *Nanoscale Materials in Chemistry*, ed Klabunde KJ (Wiley, New York). **2001**, 121–167.

[18] Bauer, C.A.; Stellacci, F.; Perry J.W. Relationship between structure and solubility of thiol-protected silver nanoparticles and assemblies. *Top. Catal.* **2008** 47:32–41.

[19] Wikipedia Commons – http://upload.wikimedia.org/wikipedia/commons/

[20] Hiemenz, Paul C. Principles of colloid and surface chemistry, 2nd ed. (Marcel Dekker, New York) **1986**, 703-722.

[21] Huang, D.; Liao, F.; Molesa, S.; Redinger, D.; Subramanian, V. Plastic-Compatible Low Resistance Printable Gold Nanoparticle Conductors for Flexible Electronics *J. Electrochem. Soc.* **2003**, *150*, G412.

[22] Pawlow P. The dependency of melting point on the surface energy of a solid body *Z. Phys. Chem.* **1909**, Vol. 65, pp. 1-25, 545-8.

[23] Buffat P.H.; Borel J.-P. Size effect on the melting temperature of gold particles. *Phys. Rev. A.* **1976**, Vol. 13, No. 6, pp. 2287-2298.

[24] Manna, A.; Imae, T.; Iida, M.; Hisamatsu, N. Formation of Silver Nanoparticles from a N-Hexadecylethylenediamine Silver Nitrate Complex. *Langmuir* **2001,** *17,* 6000-6004.